arXiv:1403.5152v1 [astro-ph.SR] 20 Mar 2014

A PLANAR JITTERING-JETS PATTERN IN CORE COLLAPSE SUPERNOVA EXPLOSIONS

Oded Papish[1] and Noam Soker[1]

ABSTRACT

We use 3D hydrodynamical numerical simulations and show that jittering bipolar jets that power core-collapse supernova (CCSN) explosions channel further accretion onto the newly born neutron star (NS) such that consecutive bipolar jets tend to be launched in the same plane as the first two bipolar jet episodes. In the jittering-jets model the explosion of CCSNe is powered by jittering jets launched by an intermittent accretion disk formed by accreted gas having a stochastic angular momentum. The first two bipolar jets episodes eject mass mainly from the plane defined by the two bipolar axes. Accretion then proceeds from the two opposite directions normal to that plane. Such a flow has an angular momentum in the direction of the same plane. If the gas forms an accretion disk, the jets will be launched in more or less the same plane as the one defined by the jets of the first two launching episodes. The outflow from the core of the star might have a higher mass flux in the plane define by the jets. In giant stellar progenitors we don't expect this planar morphology to survive as the massive hydrogen envelope will tend to make the explosion more spherical. In SNe types Ib and Ic, where there is no massive envelope, the planar morphology might have an imprint on the supernova remnant. We speculate that planar jittering-jets are behind the morphology of the Cassiopeia A supernova remnant.

1. INTRODUCTION

One class of core collapse supernova (CCSN) explosion models is based on neutrino (Colgate & White 1966), mainly the delayed neutrino mechanism (e.g., Bethe & Wilson 1985; Burrows & Lattimer 1985; Burrows et al. 1995; Fryer & Warren 2002; Ott et al. 2008; Marek & Janka 2009; Nordhaus et al. 2010; Kuroda et al. 2012; Hanke et al. 2012; Janka 2012; Bruenn et al. 2013). However, recent 3D numerical studies have shown that the desired explosions are harder to achieve (Couch 2013; Janka et al. 2013; Takiwaki et al. 2013)

[1]Department of Physics, Technion – Israel Institute of Technology, Haifa 32000, Israel; papish@techunix.technion.ac.il; soker@physics.technion.ac.il

than what 2D numerical simulations had suggested (for a summary of problems of the delayed neutrino mechanism see Papish et al. 2014). The problems of the delayed-neutrino mechanism can be overcome if there is a strong wind, either from an accretion disk (Kohri et al. 2005) or from the newly born neutron star (NS). Such a wind is not part of the delayed-neutrino mechanism, and most researchers consider this wind to have a limited contribution to the explosion.

Another class of explosion mechanisms is the jittering-jet scenario (Soker 2010; Papish & Soker 2011, 2012a,b, 2014; Gilkis & Soker 2013). Processes for CCSN explosion by jets were considered before the development of the jittering-jet scenario (e.g. LeBlanc & Wilson 1970; Meier et al. 1976; Bisnovatyi-Kogan et al. 1976; Khokhlov et al. 1999; MacFadyen et al. 2001; Höflich et al. 2001; Woosley & Janka 2005; Burrows et al. 2007; Couch et al. 2009, 2011; Lazzati et al. 2011). However, most of these MHD models require a rapidly spinning core before collapse starts, and hence are limited to a small fraction of all CCSNe. The jittering-jet scenario posits that *all CCSNe are exploded by jets*. Recent observations (e.g. Milisavljevic et al. 2013; Lopez et al. 2013; Ellerbroek et al. 2013) show indeed that jets might have a much more general role in CCSNe than what is expected in the neutrino-driven mechanisms and mechanisms that require rapidly rotating cores.

In the jittering-jets scenario the sources of the angular momentum for disk formation are the convective regions in the core (Gilkis & Soker 2013) and instabilities in the shocked region of the collapsing core, e.g., neutrino-driven convection or the standing accretion shock instability (SASI). Recent 3D numerical simulations show indeed that neutrino-driven convection and SASI are well developed in the first second after core bounce (Hanke et al. 2013; Takiwaki et al. 2013) and the unstable spiral modes of the SASI can amplify magnetic fields (Endeve et al. 2012). The spiral modes with the amplification of magnetic fields build the ingredients necessary for jets' launching.

When the average specific angular momentum of the matter in the pre-collapse core is small relative to the amplitude of the specific angular momentum of these instabilities, intermittent jets-launching episodes with random directions occur. The two launching axes of the first two launching episodes define a plane. Using the FLASH numerical code we set a numerical study of the accretion pattern that is likely to be formed after the first two launching episodes. The code and numerical set-up for the 3D simulations are described in section 2. The accretion pattern following two jets-launching episodes, followed by a third episode, is described in section 3. Our summery is in section 4.

2. NUMERICAL SETUP

We study the accretion structure that result from multiple jets-launching episodes using the FLASH gasdynamical numerical code version 4.2 (Fryxell et al. 2000). The widely used FLASH code is a publicly available code for supersonic flow suitable for astrophysical applications.

The simulations are done using the split PPM solver of FLASH. We use 3D Cartesian coordinates with an adaptive mesh refinement (AMR) grid. The grid is divided into two regions similar to Papish & Soker (2014). (1) A spherical inner region with a radius of about 1000 km. Inside this region we set the maximum refinement level to be proportional to angular size. This is up to a radius of ~ 300 km where the maximum refinement level is constant and with a resolution of about 6 km. (2) In the region outside 1000 km we set a constant maximum refinement level which coincides with the maximum refinement level at the outer boundary of the inner region; the resolution in the outer region is ~ 15 km. This separation into two different regions enables us to simulate both the region near the NS where we inject the jets and the large scale regions where the jets interact with the surrounding core material. The total size of the grid is $10,000 \times 20,000$ km. We treat the spherical inner region of up to 75 km from the center as a hole. This means that we are not simulating the NS itself, nor the assumed accretion disk. The boundary condition at the edge of the hole is inflow only, meaning the velocity cannot be positive in the radial direction unless we inject a jet at that specific zone.

We start the simulations after the core has collapsed and bounced back. The initial conditions are taken for a $15 M_{\odot}$ model from the 1D simulations of Liebendörfer et al. (2005) at a time of $t \simeq 0.2$ s after bounce. We map their results into 3D, including the chemical composition. We set outflow boundary conditions at the exteriors of the simulation's domain.

In each episode we inject one pair of two opposite jets (bipolar jets). All jets' axes are in one plane, that we take to be the $y = 0$ plane of the numerical Cartesian grid. We take the z axis of the numerical grid to be at 40° to the direction of the symmetry axis of the first jets pair. The n launching episode results in two opposite jets at some angle θ_n from the direction of the first jets. All jets have an initial conical shape, with a half opening angle of 10°.

3. ACCRETION PATTERN

3.1. Simulated Cases

We start each simulation by injecting two opposite jets, the first jets' launching episode. The second bipolar jets pair is injected either at an angle of 40° or 70° relative to the first episode. Each jet launching episode lasts 0.05 s, and the second episode is launched immediately after the end of the first episode. The different simulated cases are summarized in Table 1. The direction of the jets launched in the first two episodes are presented in Fig. 1. Note that in that presentation one of the jets in each pair is represented by two regions.

Run	θ_1	θ_2	θ_3
Active(s)	$0-0.05$	$0.05-0.1$	$0.1-0.15$
A1	0°	40°	80°
A2	0°	40°	−40°
B1	0°	70°	55°
B2	0°	70°	110°

Table 1:: A1, A2, B1, and B2 are the three different simulated cases. The angles θ_2 and θ_3 are the angles of the jets in the second and third jets' launching episodes relative to the direction of the first jets that are injected at 40° from the z axis. All jets are injected in the $y = 0$ plane. Each episode lasts 0.05 s.

3.2. First jet-launching episode

In Fig. 2 we present the density, left panel, and the velocity and temperature, right panel, maps at the end of the first jets launching episode. The flow structure has the typical structure of jet-inflated bubbles (see review by Soker et al. 2013). Here we should note the following. (i) The jets shock material to high temperatures and densities, where nucleosynthesis takes place. These regions have high velocities and can have imprint on the distribution of different isotopes in the SN remnant at later times. This will not be studied here. (ii) The pre-jets flow is that of a collapsing core onto a newly formed NS. After the first jets launching episode accretion continues from directions near the plane perpendicular to the jets' axis.

Let us elaborate on the accretion pattern. In Fig. 3 we present the inflow mass flux on spheres of radii 500 and 1000 km. We present the local mass inflow rate $\dot{M}_{\rm loc}$, defined as if

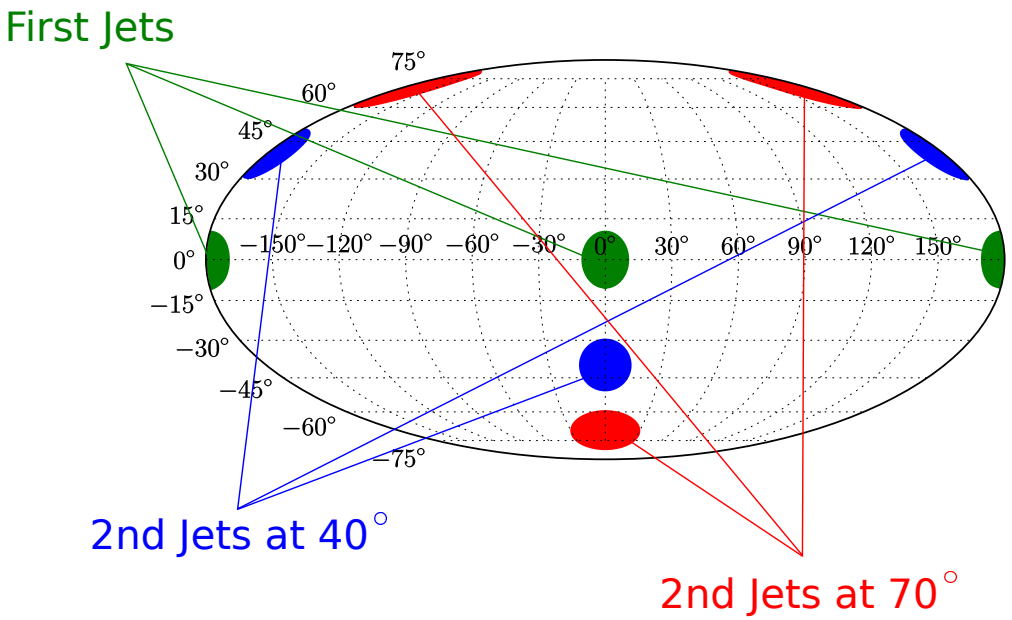

Fig. 1.—: The simulations grid in the Mollweide projection. Shown are the directions of the first and second episodes in the different Runs. In each episode two opposite jets are launched. One of the jets in each episode is represented by two halves in this diagram.

the entire sphere would have the same inflow mass flux as in the given location,

$$\dot{M}_{\rm loc} = 4\pi r^2 \rho v_{\rm in}, \tag{1}$$

where ρ and $v_{\rm in}$ is the density and the radial inward velocity at the point. The first jets pair is able to penetrate thorough the inflowing matter to beyond 1000 km (Papish & Soker 2014). As the jets gas is in outflow, it appears as white areas in Fig. 3 and the following similar figures.

3.3. A bipolar accretion pattern

We run two cases of a second jets-launching episode, in directions of 40° (Run A) and 70° (Run B) relative to the direction of the jets' axis in the first episode. All jets' axes are in the $y = 0$ plane. The density maps, left panels, and the temperature maps with velocity arrows, right panels, of the two cases at the end of the second episode, $t = 0.1$ s, are presented in Fig. 4. All plots are in the $y = 0$ plane. From these panels, two for each Run, we learn that the strongest inflow is from two opposite directions, through which we draw a dashed line on the density maps of the figure at angles of $\alpha_1 = 35°$, and $\alpha_2 = 54°$ respectively relative to the x-axis.

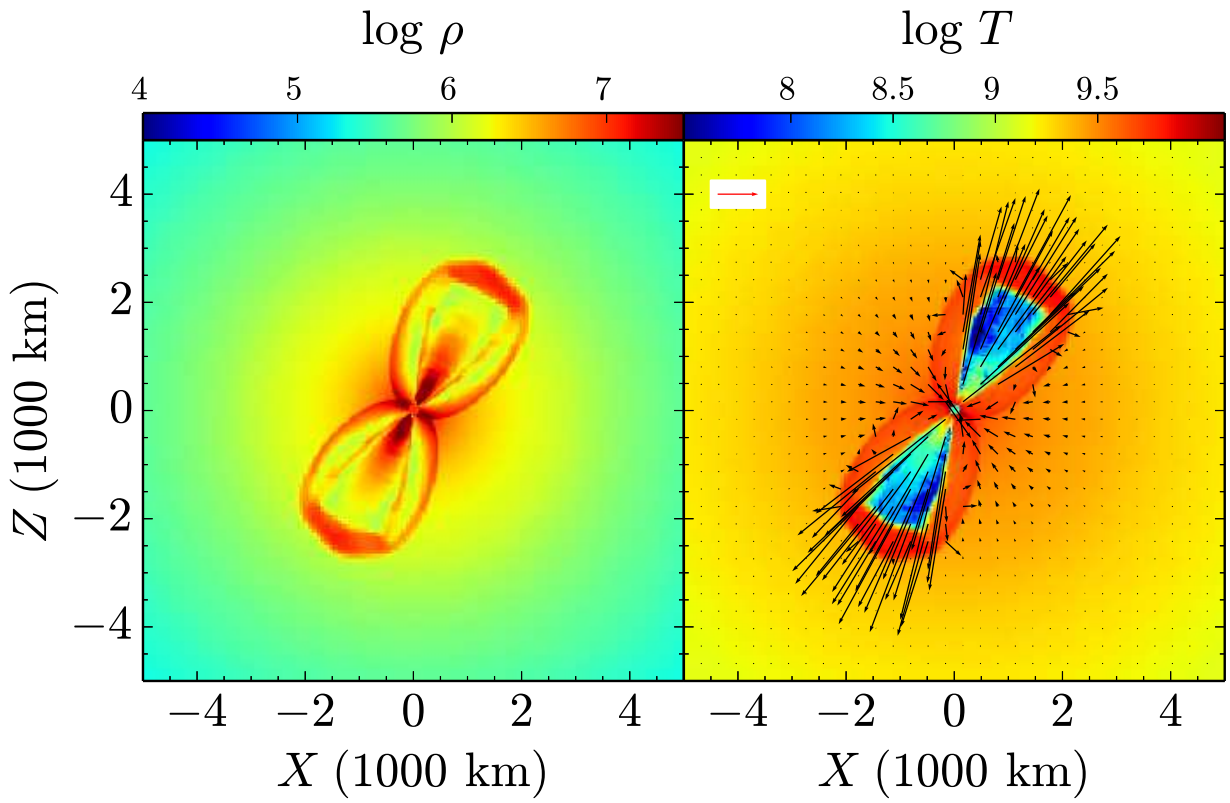

Fig. 2.—: Flow pattern in the $y = 0$ plane at the end of the first jets launching episode ($t = 0.05$ s), common to all simulated cases. Left Panel: density, with a color coding in logarithmic scale and units of g cm^{-3}. Right Panel: temperature in log scale and in units of K, and a velocity map. Velocity is proportional to the arrow length, with inset showing an arrow for $30,000$ km s^{-1}.

To identify the inflow pattern of the gas, most of which will be eventually accreted by the NS, we present in Fig. 5 the flow structure in a plane perpendicular to the $y = 0$ plane, and cutting it along the dashed lines drawn in the density maps of Fig. 4. Note that the two planes for Run A and Run B are not identical. The left panels of Fig. 5 present the density maps of the two Runs, while the right panels present the inflow mass flux and flow velocity maps. The mass flux is $\dot{M}_{\rm loc}$ as define in equation (1). In is evident that the inflow close to the NS at the center is mainly from two general opposite directions, the $+y$ and $-y$ directions, that are perpendicular to the axes of the two jets' launching episodes. When the angle between the two first jet-pairs is small, 40°, the high inflow mass flux is from two extended opposite areas. These becomes smaller when the angle between the two episodes are large, 70°. A bipolar accretion flow pattern has emerged.

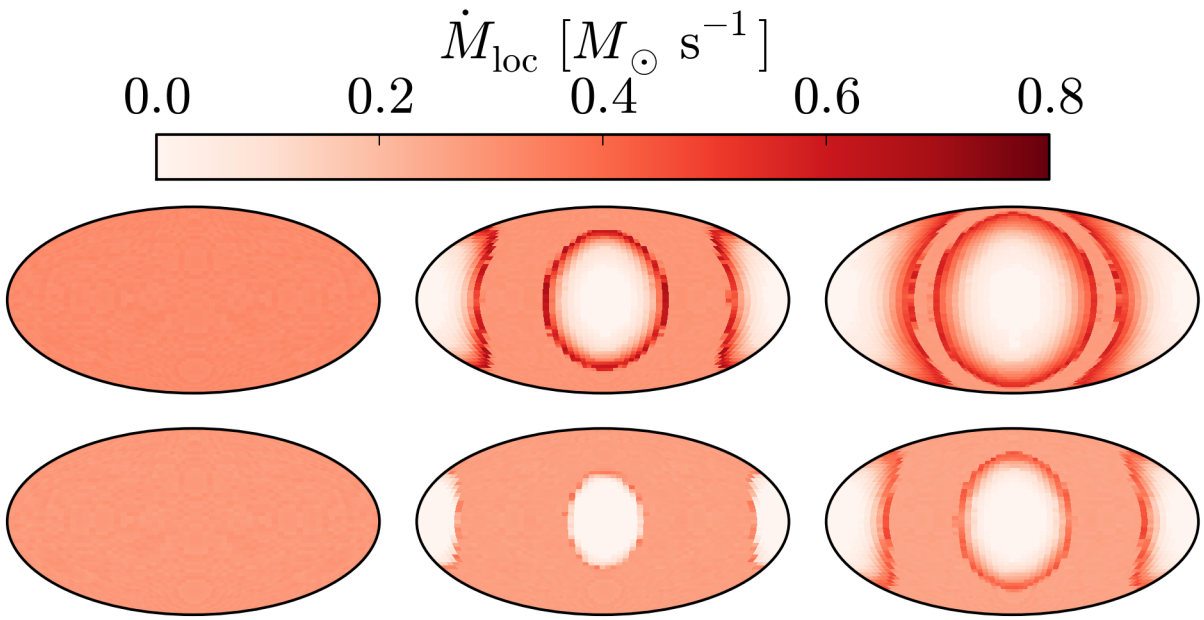

Fig. 3.—: The inflow mass flux at times $t = 0, 0.026, 0.05$ s, i.e., at the beginning, middle and end of the first jets-launching episode, given on spheres of radius $r = 500$ km (upper row) and $r = 1000$ km (lower row). Mass inflow rate at each point is calculated as if the entire sphere would have the same inflow mass flux as in the given point (eq. 1). White areas are regions with outflow, i.e., the jets.

We can also use the Mollweide-projection (see Fig. 1) to present the emergence of the bipolar inflow (accretion) pattern. This is shown in Fig. 6 for Run A, and in Fig. 7 for Run B. Presented are the inflow mass fluxes on spheres of radii 500 km and 1000 km, as in Fig. 3 for the first jets. Again, the emergence of a bipolar inflow (accretion) structure is evident, particularly in Run B presented in Fig. 7.

3.4. Later evolution

As we discussed in the next section, jets launched by accretion disks formed from the bipolar accretion pattern are likely to be lunched perpendicular to the direction of accretion. Namely, they will be launched in, or close to, the $y = 0$ plane defined by the jets' axes of the first two episodes. We are not in the numerical stage to follow the angular momentum of the accreted gas and from that to find the direction to launch the next jets episode. We

therefore arbitrarily run 4 cases for the third jets launching episode as listed in Table 1. In all these cases the third jets launching episode is active in the time period $t = 0.1 - 0.15$ s. We present the flow structure for two cases, A1 and B2, in Fig. 8, at the end of the active phase $t = 0.15$ s. In all cases we find that a third jets-launching episode strengthens the bipolar accretion pattern and the inflow becomes further concentrated to two opposite directions. In Fig. 9 we use the Mollweide-projection (see Fig. 1) to present the inflow rates through a spheres of radius $r = 500$ km for the four Runs at the end of the third episode. The jets of the third episode make the bipolar accretion pattern more prominent.

To further quantify the bipolar accretion pattern we construct two opposite cones whose common vertex is at the center, and calculate the ratio of the average inflow mass flux through the cones to the average inflow mass flux through the entire sphere at the same radius. The cones' axis is perpendicular to the $y = 0$ plane, i.e., perpendicular to the jets' axes, and through the center. The quantity we use is

$$\xi \equiv \frac{\dot{M}_{\rm cone}({\rm inflow})/\Omega}{M_{\rm total}({\rm inflow})/4\pi}, \tag{2}$$

where Ω is the solid angle covered by the two cones. The evolution of ξ with time for two cone-pairs and at two radii are presented in Fig. 10, for the 4 different Runs listed in Table 1. In one cones pair each cone has an opening angle of 30°, and in the other each cone has an opening angle of 45°. We note that the flow becomes more concentrate, i.e., ξ increases with time, to the perpendicular direction as more jets are launched in the $y = 0$ plane. The mass flux per unit solid angle for the 30° cones is substantially larger than that for the 45° cones, $\xi(30^\circ) > \xi(45^\circ)$. This implies that the inflow has the pattern of two opposite stream columns. This is what we refer to as a bipolar accretion pattern. We next turn to discuss the implication of the bipolar accretion pattern.

4. IMPLICATIONS AND SUMMARY

In this study we assumed that CCSN explosions are driven by jittering-jets (Papish & Soker 2011), an examined the pattern by which jets are launched. The angular momentum of the core is not large, such that the jets' axis is determined, at least in part, by stochastic processes such as instabilities and convection in the pre-collapse core (Gilkis & Soker 2013). We conducted 3D numerical simulations with the FLASH code (Fryxell et al. 2000). In each jets-launching episode we launched one pair of bipolar jets (Fig. 2). Under these assumptions, the directions of the two first jets-launching episode are more or less random. However, the first two episodes, if not along the same direction, define a plane. We set this plane to be $y = 0$ in our study. The jets will eject mass outward along their propagation direction,

leaving inflow in perpendicular directions. After the first episode the inflow is from a belt region perpendicular to the jets' axis, as demonstrated in Fig. 3. After the second episode the inflow is concentrated in two opposite directions, as clearly seen in Figs. 5, 6 and 7. A bipolar accretion flow with its axis perpendicular to the $y = 0$ plane has been formed.

An inflowing gas along a direction normal to the $y = 0$ plane has an angular momentum direction within that plane. This implies that bipolar accretion flow makes it more likely that the axis of the jets in the third episode will be in the $y = 0$ plane, as jets are launched along the angular momentum axis. Namely, the third episode jets' axis will be in about the same plane as the axes of the first two episodes.

We simulated two directions for the second jets episode, and for each of these we simulated two directions in the same plane for a third jets episode. These four cases are summarized in Table 1. The asymmetry in the accretion flow is presented for these cases in Fig. 10, quantified by the the parameter ξ defined in equation (2). The bipolar pattern becomes more prominent as the inflow becomes more concentrated along two opposite directions. This implies that the following launching of jets will be in, or near, the $y = 0$ plane.

The bubbles inflated by the jets grow and expand to all directions as they move toward lower density core gas. Eventually they will close on directions perpendicular to their axis as well, and expel the outer core and the rest of the star in all directions. In addition, some of the jets will not be exactly in the same plane, but will have some stochastic variations from the $y = 0$ plane. This will also help in expelling the rest of the star in all directions. This later evolutionary phase will be studied in the future.

Can this *planar jittering pattern* have any observational consequences? We don't expect prominent signature in in Type II SNe where the shock will become more spherical as it propagate through the extended massive hydrogen envelope. In type Ic SNe the imprint might exist in the supernova remnant (SNR). We raise here the possibility that the torus morphology of a tilted thick disk with multiple jets in Cassiopeia A SNR (DeLaney et al. 2010; Milisavljevic & Fesen 2013) is a result of a planar jittering pattern. The last jet was more free to expand, as all core has been removed, and it is now observed as the high velocity jet like outflow along the northeast direction of the SNR.

Finally, we point out that a planar jet launching patter might have taken place during galaxy formation, where a feedback between accretion of cold gas and jet activity might have taken place.

This research was supported by the Asher Fund for Space Research at the Technion, and a generous grant from the president of the Technion Prof. Peretz Lavie. OP is supported by the Gutwirth Fellowship.

REFERENCES

Bethe, H. A., & Wilson, J. R. 1985, ApJ, 295, 14

Bisnovatyi-Kogan, G. S., Popov, I. P., & Samokhin, A. A. 1976, Ap&SS, 41, 287

Bruenn, S. W., Mezzacappa, A., Hix, W. R., et al. 2013, ApJ, 767, L6

Burrows, A., & Lattimer, J. M. 1985, ApJ, 299, L19

Burrows, A., Hayes, J., & Fryxell, B. A. 1995, ApJ, 450, 830

Burrows, A., Dessart, L., Livne, E., Ott, C. D., & Murphy, J. 2007, ApJ, 664, 416

Colgate, S. A., & White, R. H. 1966, ApJ, 143, 626

Couch, S. 2013, Presented in the Fifty-one erg meeting, Raleigh, May 2013.

Couch, S. M., Pooley, D., Wheeler, J. C., & Milosavljević, M. 2011, ApJ, 727, 104

Couch, S. M., Wheeler, J. C., & Milosavljević, M. 2009, ApJ, 696, 953

DeLaney, T., Rudnick, L., Stage, M. D., et al. 2010, ApJ, 725, 2038

Ellerbroek, L. E., Podio, L., Kaper, L., et al. 2013, A&A, 551, A5

Endeve, E., Cardall, C. Y., Budiardja, R. D., Beck, S. W., Bejnood, A., Toedte, R. J., Mezzacappa, A., & Blondin, John M.. 2012, ApJ, 751, 26

Fryer, C. L., & Warren, M. S. 2002, ApJ, 574, L65

Fryxell, B., Olson, K., Ricker, P., et al. 2000, ApJS, 131, 273

Gilkis, A., & Soker, N. 2013, submitted

Hanke, F., Marek, A., Müller, B., & Janka, H.-T. 2012, ApJ, 755, 138

Hanke, F., Müller, B., Wongwathanarat, A., Marek, A., & Janka, H.-T. 2013, arXiv:1303.6269

Höflich, P., Khokhlov, A., & Wang, L. 2001, 20th Texas Symposium on relativistic astrophysics, 586, 459

Janka, H.-T. 2012, Annual Review of Nuclear and Particle Science, 62, 407

Janka et al. 2013, Presented in the Fifty-one erg meeting, Raleigh, May 2013.

Khokhlov, A. M., Höflich, P. A., Oran, E. S., et al. 1999, ApJ, 524, L107

Kohri, K., Narayan, R., & Piran, T. 2005, ApJ, 629, 341

Kuroda, T., Kotake, K., & Takiwaki, T. 2012, ApJ, 755, 11

Lazzati, D., Morsony, B. J., Blackwell, C. H., & Begelman, M. C. 2011, arXiv:1111.0970

LeBlanc, J. M., & Wilson, J. R. 1970, ApJ, 161, 541

Liebendörfer, M., Rampp, M., Janka, H.-T., & Mezzacappa, A. 2005, ApJ, 620, 840

Lopez, L. A., Ramirez-Ruiz, E., Castro, D., & Pearson, S. 2013, ApJ, 764, 50

MacFadyen, A. I., Woosley, S. E., & Heger, A. 2001, ApJ, 550, 410

Marek, A., & Janka, H.-T. 2009, ApJ, 694, 664

Meier, D. L., Epstein, R. I., Arnett, W. D., & Schramm, D. N. 1976, ApJ, 204, 869

Milisavljevic, D., Soderberg, A., Margutti, R., et al. 2013, arXiv:1304.0095

Milisavljevic, D., & Fesen, R. A. 2013, ApJ, 772, 134

Nordhaus, J., Burrows, A., Almgren, A., & Bell, J. 2010, ApJ, 720, 694

Ott, C. D., Burrows, A., Dessart, L., & Livne, E. 2008, ApJ, 685, 1069

Papish, O., & Soker, N. 2011, MNRAS, 1321

Papish, O., & Soker, N. 2012a, Death of Massive Stars: Supernovae and Gamma-Ray Bursts, 279, 377

Papish, O., & Soker, N. 2012b, MNRAS, 421, 2763

Papish, O., & Soker, N. 2014, MNRAS, 438, 1027

Papish, O., Nordhaus, J., & Soker, N. 2014, arXiv:1402.4362

Soker, N. 2010, MNRAS, 401, 2793

Soker, N., Akashi, M., Gilkis, A., et al. 2013, Astronomische Nachrichten, 334, 402

Takiwaki, T., Kotake, K., & Suwa, Y. 2013, arXiv:1308.5755

Woosley, S., & Janka, T. 2005, Nature Physics, 1, 147

This preprint was prepared with the AAS LaTeX macros v5.2.

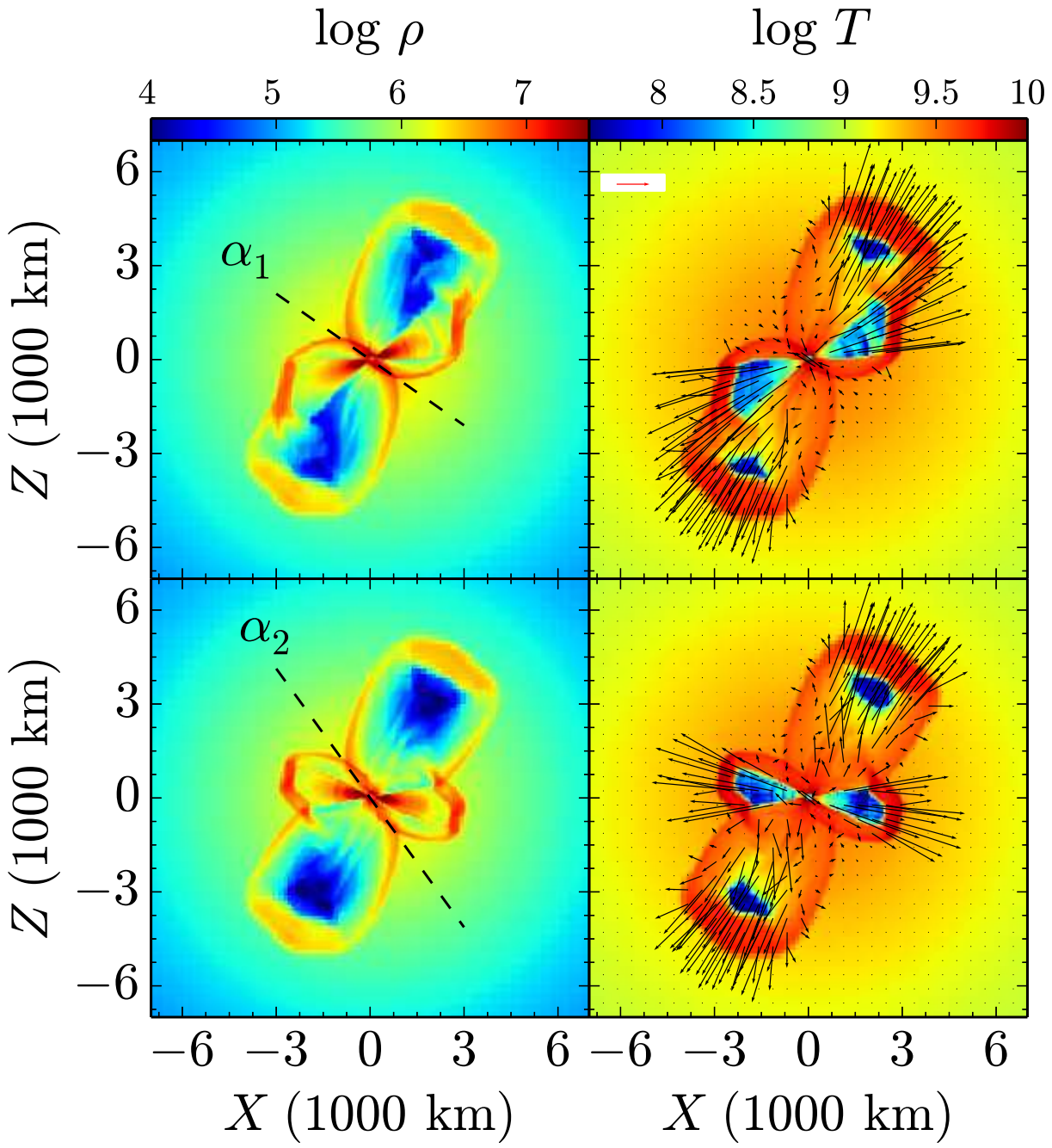

Fig. 4.—: Flow structure at the end of the second jets episode at $t = 0.1$ s in the $y = 0$ plane, for Run A in the upper panels, and for Run B in the lower panels. Left Panels: density, with a color coding in log scale and units of g cm^{-3}. The dashed line indicate the intersect of the plane shown in Fig. 4. Right Panels: temperature in log scale in units of K, and velocity arrows. Velocity is proportional to the arrow length, with inset showing an arrow for $30,000$ km s^{-1}.

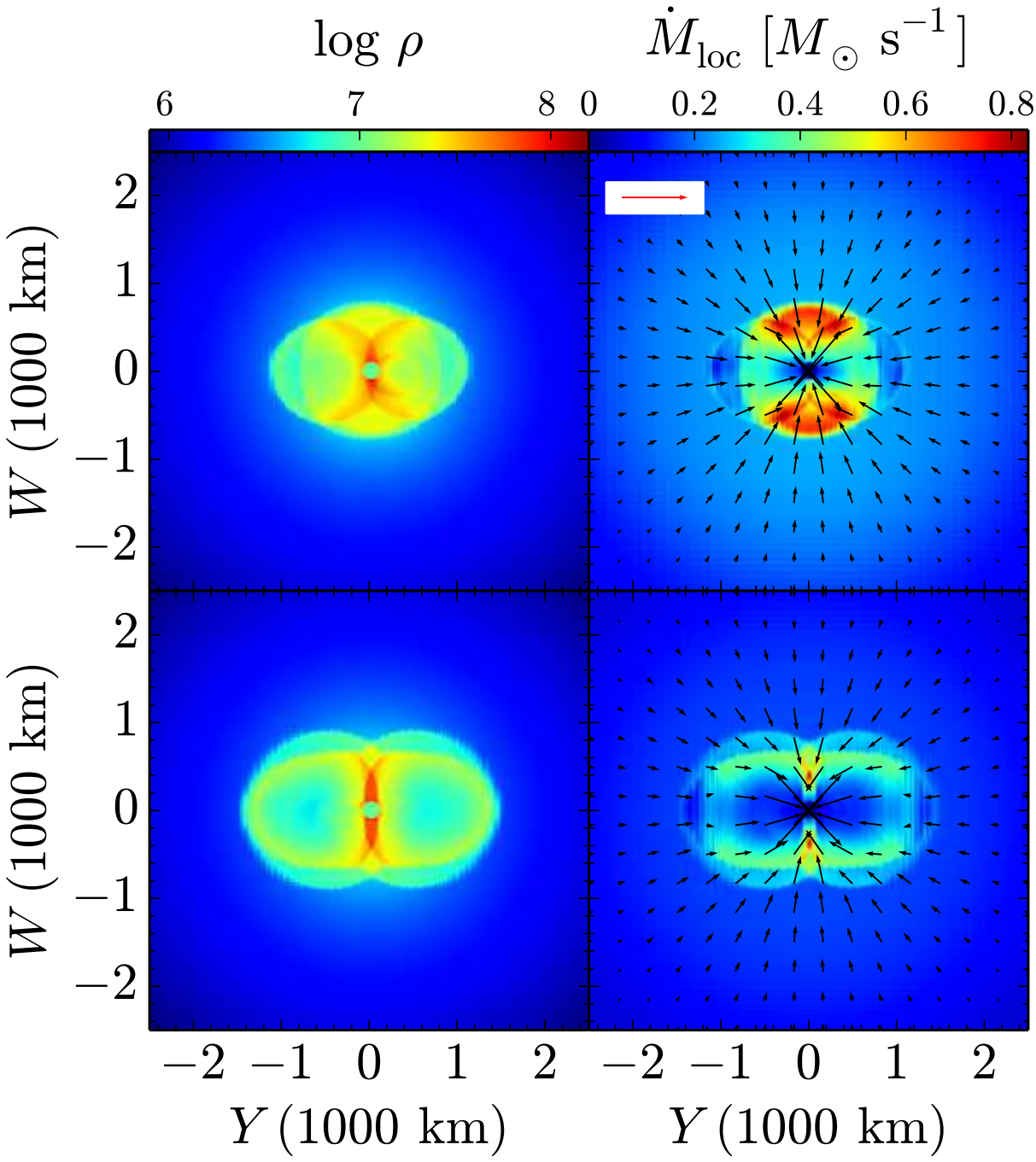

Fig. 5.—: Flow structure at the end of the second jets episode at $t = 0.1$ s, as in Fig. 4, but in a plane perpendicular to the $y = 0$ plane and intersecting it at the dashed line drawn on the left panels of Fig. 4. The coordinate along the dashed line is define as W, and it is along the line $z = -0.7x$ for Run A (upper panels) and $z = -1.38x$ for Run B (lower panels). Note that the panels here show a small inner region of the grid. Partition of panels as in Fig. 4, but in the right panels the color represent mass influx rate $\dot{M}_{loc}$.

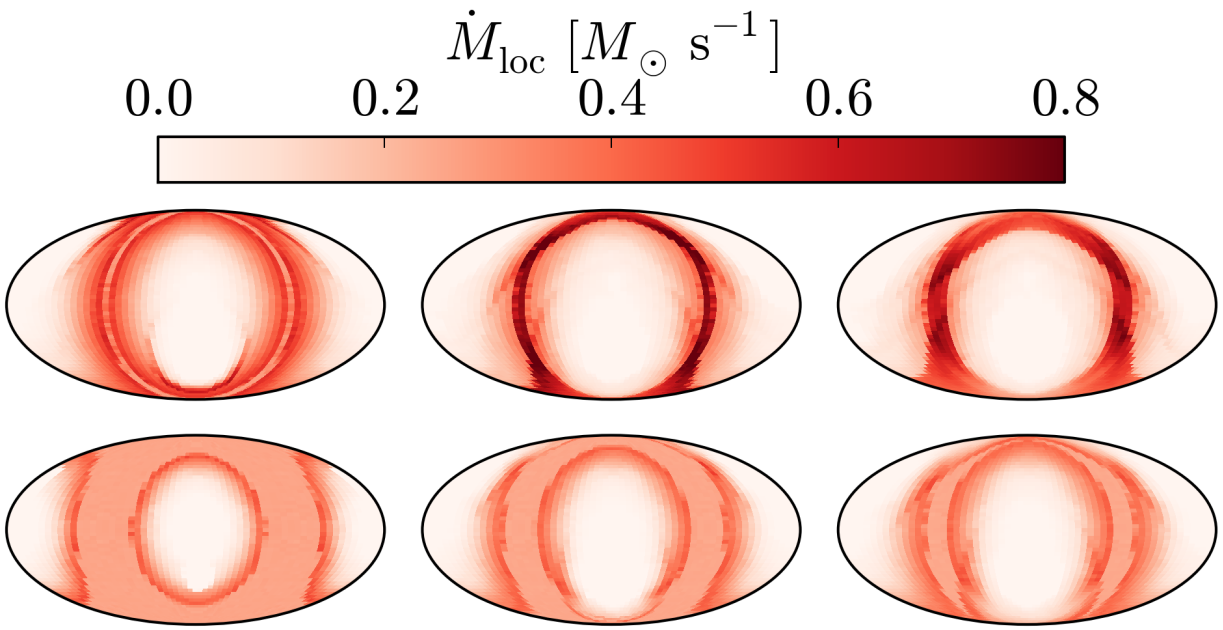

Fig. 6.—: The inflow mass flux at $t = 0.062, 0.084, 0.1$ s, from left to right, i.e., at the beginning, middle and end of the second jets-launching episode, for Run A, given on spheres of radius $r = 500$ km (upper row) and $r = 1000$ km (lower row). Mass inflow rate at each point is calculated as if the entire sphere would have the same inflow mass flux as in the given point (eq. 1. White area are regions no inflow, some with outflow, i.e., the jets. Note the emergence of two opposite high accretion rate regions.

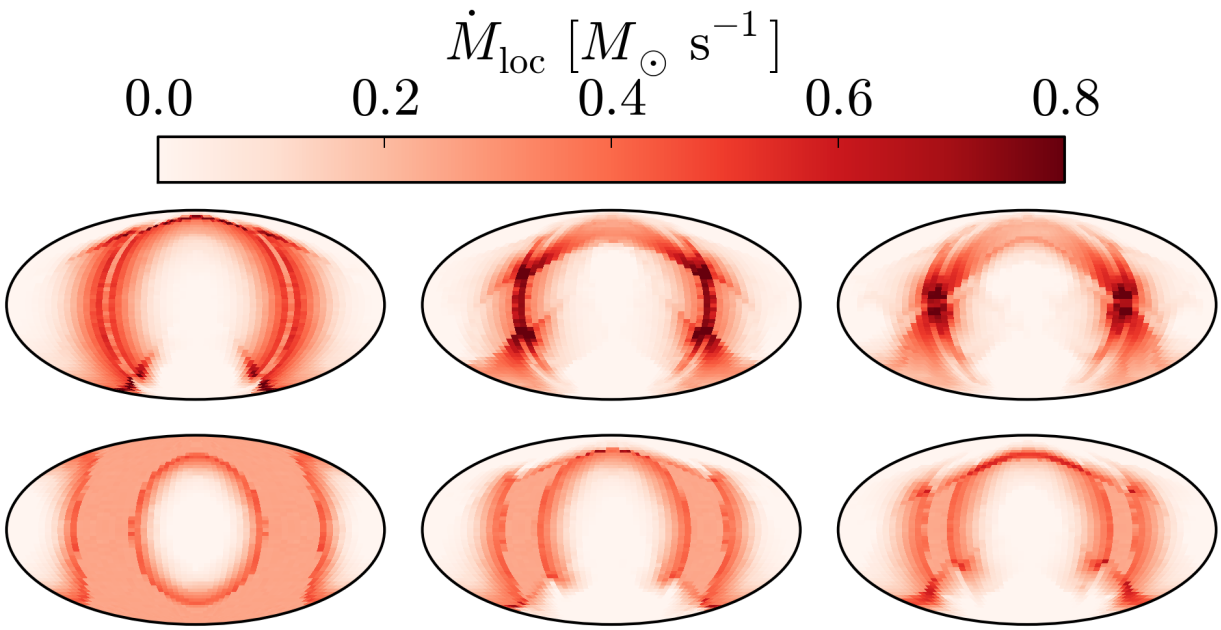

Fig. 7.—: Like Fig. 6, but for Run B, where the jets of the second episode are launched at $\theta_1 = 70°$ to the first jets' axis, rather than $\theta_1 = 40°$. The bipolar accretion patter is clearly seen in the dark-red areas.

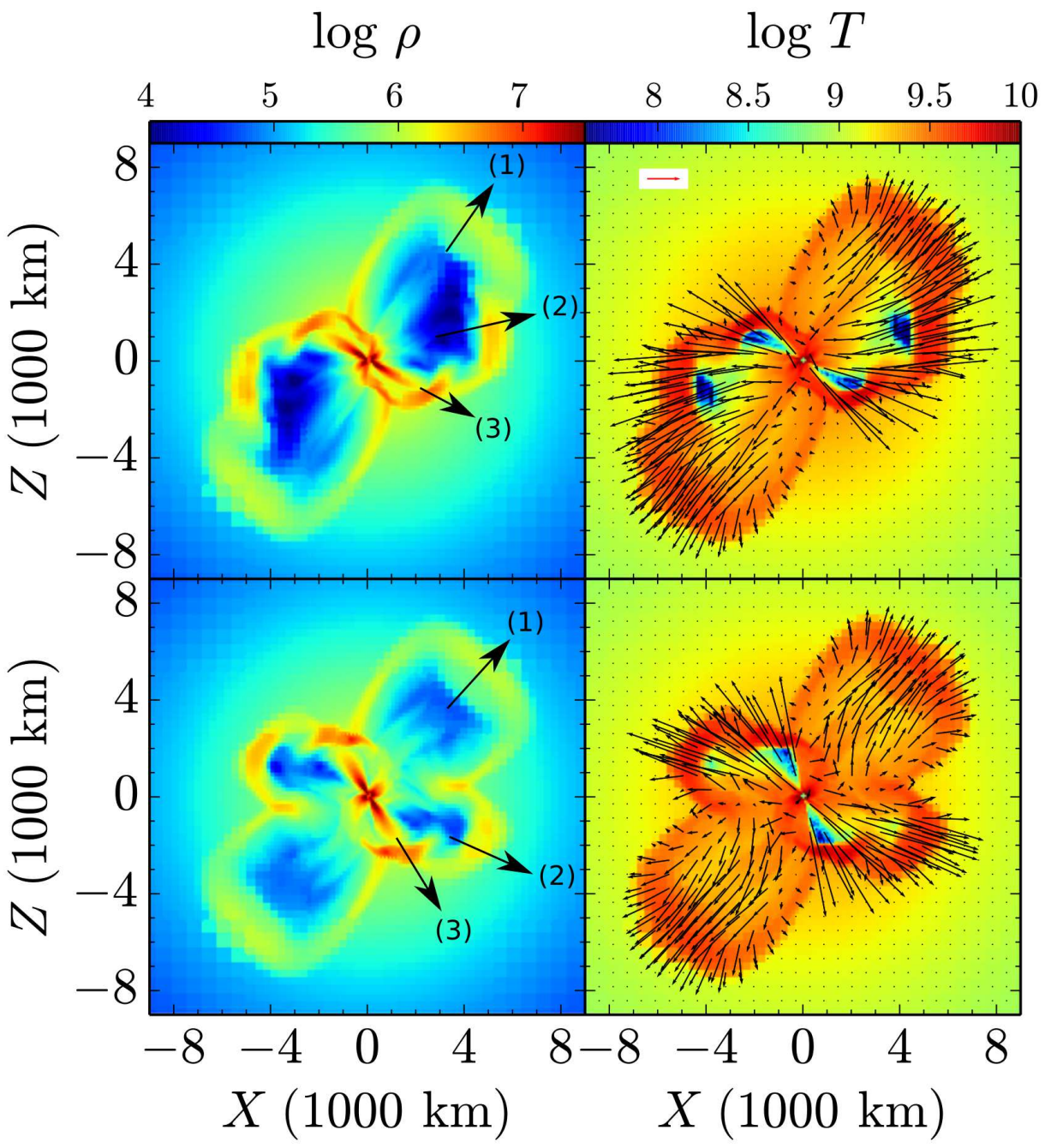

Fig. 8.—: Flow structure in the $y = 0$ plane at the end of the third jets launching episode, $t = 0.15$ s, for Run A1 (upper panels) and B2 (lower panels). Left Panels: density, with a color coding in logarithmic scale and units of g cm^{-3}. The three arrows depict the direction of jets' launching in the three episodes as numbered. Right Panels: temperature in log scale in units of K, and velocity map. Velocity is proportional to the arrow length, with inset showing an arrow for 30, 000 km s^{-1}.

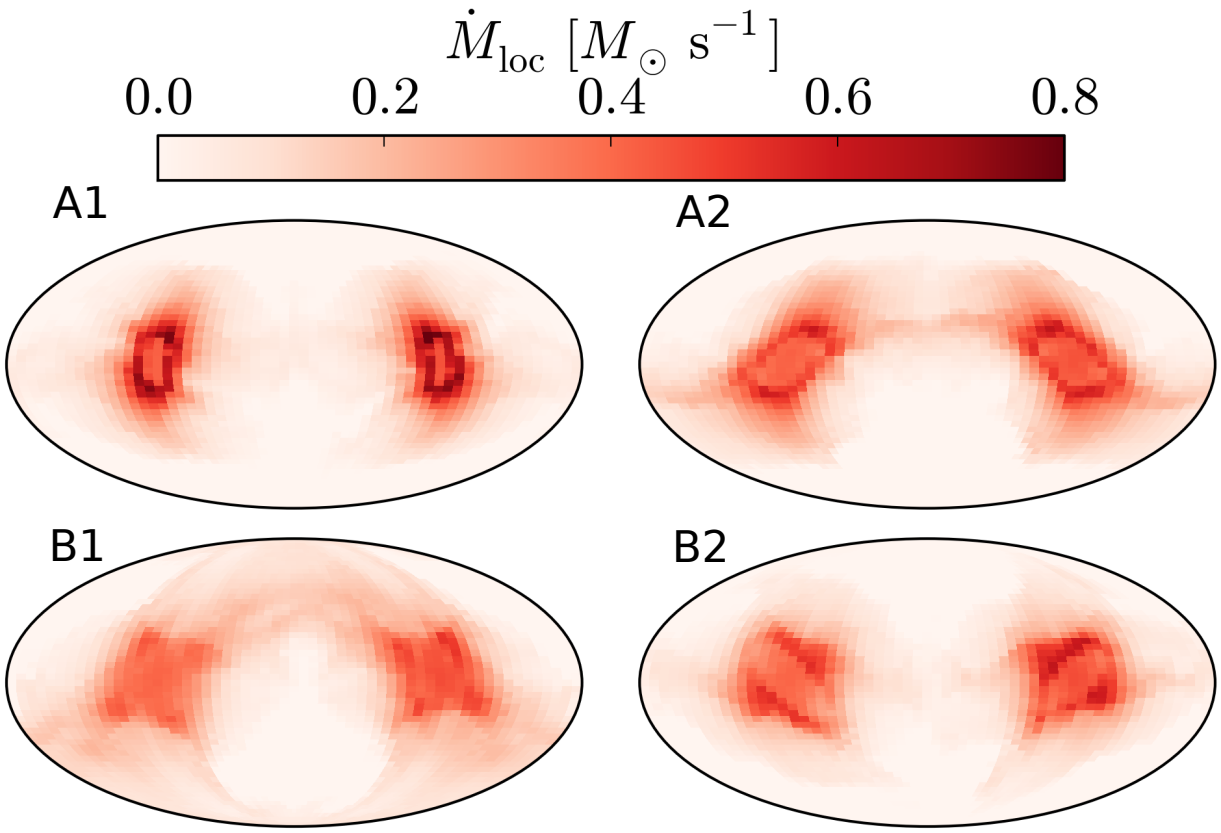

Fig. 9.—: Like Fig. 6 but at $t = 0.15$ s and on a sphere of radius $r = 500$ km. The four cases are as indicated on the panels and according to Table 1. The third jets episode strengthens the bipolar accretion pattern.

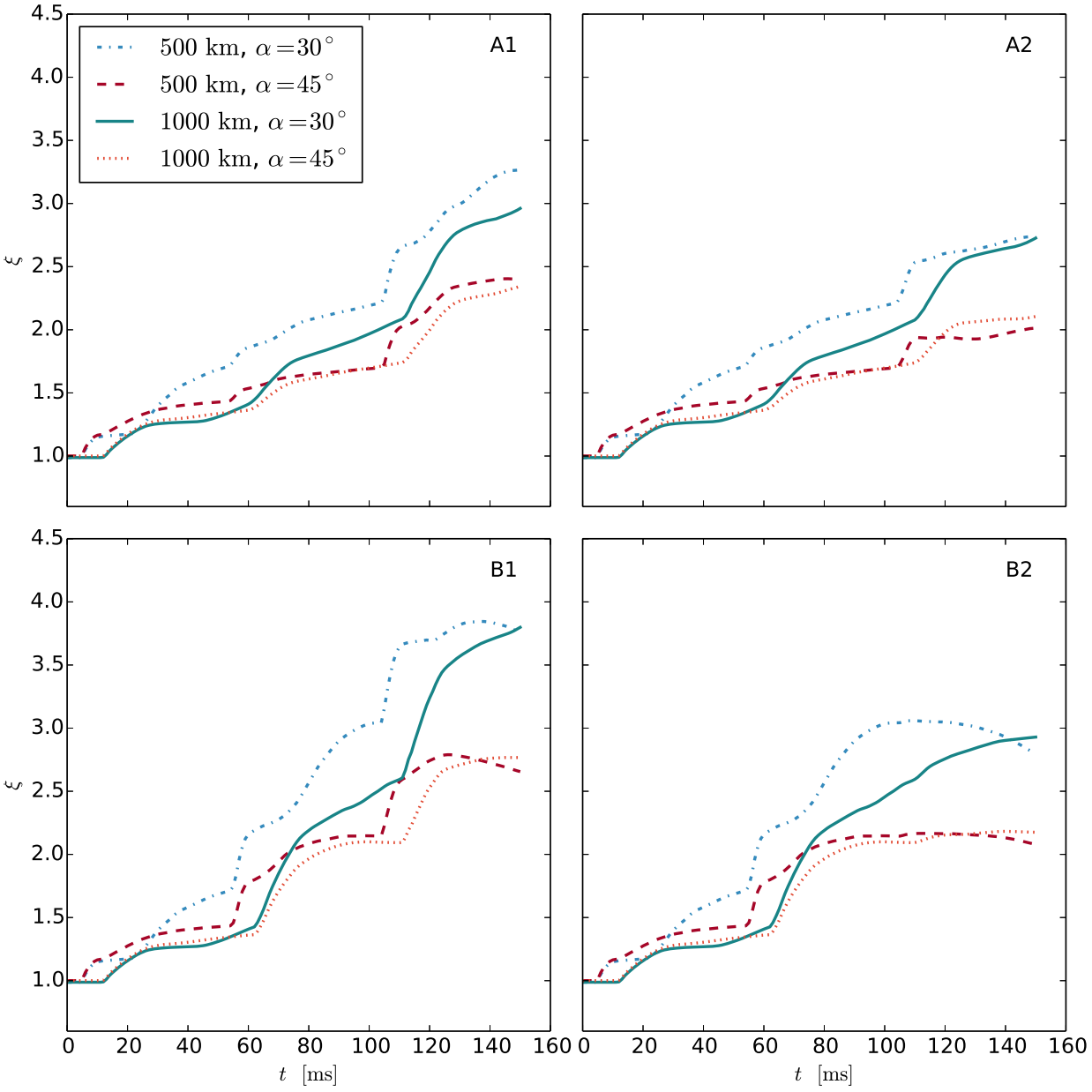

.

Fig. 10.—: The normalized mass inflow rate ξ, as given in equation 2, within two opposite cones of opening angle α and at two radii. The four cases marked are according to Table 1.